ACS APPLIED MATERIALS & INTERFACES

Letter

www.acsami.org

Improving Pore Filling of Gel Electrolyte and Charge Transport in Photoanode for High-Efficiency Quasi-Solid-State Dye-Sensitized Solar Cells

Baohua Wang, Shuai Chang, Lawrence Tien Lin Lee, Shizhao Zheng, King Yong Wong, Quan Li, Xudong Xiao, and Tao Chen*

Department of Physics, The Chinese University of Hong Kong, Shatin, Hong Kong SAR, China

Supporting Information

ABSTRACT: We demonstrate the enhancement of pore-filling and wettability of gel electrolyte in quasi-solid-state dye-sensitized solar cells (DSSCs) by developing a kinetically driven electrolyte infiltration approach, in which the air purging provides the driving force. This method renders fast electrolyte diffusion throughout the three-dimensional TiO_2 nanoparticle network, promising for large-area device fabrication. In addition, for the first time we incorporate multiwalled carbon nanotubes into the anode of quasi-solid-state DSSCs to improve the charge transfer efficiency and fill factor. These advancements finally generate an efficiency exceeding 7.0%, much higher than the device efficiency of 5.5% fabricated by the conventional method.

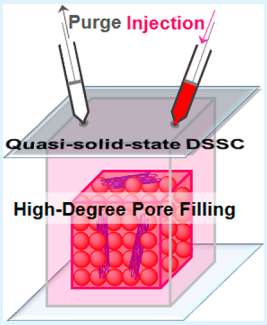

KEYWORDS: *dye-sensitized solar cell, gel electrolyte, pore filling, ion transport, carbon nanotube, electrode*

Dye-sensitized solar cells (DSSCs) have attracted intense interest because of their low-cost fabrication, color selectivity, and potential applications in building integrated photovoltaics.[1−3] Basically, upon light illumination, the photoexcited dye molecules inject electrons into the conduction band of the supporting oxide. Dye is regenerated via the reaction with reducing species (such as I^-) in the electrolyte. Efficient dye regeneration requires the dye molecule layer sufficiently wetted by the electrolyte. In addition, fast diffusion of redox shuttles between two electrodes is critical for sufficient amount of reducing species approaching dye molecules. Redox couple transportation in liquid media is efficient due to the nearly free ionic diffusion,[4] which generated benchmark efficiencies in liquid electrolyte based DSSCs during the past few decades.[5−8] However, the (volatile) solvent in liquid electrolyte usually results in leakage and/or evaporation, which are considered as one of the critical factors that shorten the lifetime of the DSSCs.[9] In this regard, (quasi-) solid-state electrolytes offer promising alternatives for the fabrication of DSSCs with long-term stability;[10] they can avoid the electrolyte leakage/evaporation and corrosion on counter electrode as well as suppress dye dissociation from oxide surface to the electrolyte.[1]

Polymer gel-based electrolyte is a class of quasi-solid-state redox transporting media, it becomes fluidic at high temperature (e.g., around 90 °C),[10−12] allowing the electrolyte injection compatible with liquid counterpart. However, a fact is that the viscosity of gel electrolyte is much larger than the liquid counterparts; the mobility of redox ions in gel electrolyte is generally a quarter of that in liquid phase.[13,14] The infiltration of gel electrolyte into the mesoporous anode network thus becomes difficult, especially for the deeper pores in the thick anode films. Moreover, it poses a great challenge in terms of large-area device fabrication. On the other hand, the existence of air inside the film can also influence the degree of pore filling and wettability of electrolyte with the dye layer.

Herein, an injecting-while-purging electrolyte injection process is developed. Two holes predrilled in the counter electrode are used for simultaneous injection of electrolyte and purge of air (Figure 1a). This approach possesses two advantages: (1) the purging process can evacuate air in the dye layer and thus improve the wettability, and (2) the air evacuation drives a fast permeation of the gel electrolyte throughout the anode film, ensuring a high degree of pore filling before the gel electrolyte cooling down. This latter advancement is especially important for large-area device fabrication. To further improve the device efficiency, we incorporate multiwalled carbon nanotube (MWCNT) into the TiO_2 network to enhance the charge transfer and ion diffusion efficiency (Figure 1b). Comparative studies show that device fabricated by injecting-while-purging protocol in the presence of MWCNT incorporation generates a high power conversion efficiency (PCE) of 7.1%, the device without MWCNT incorporation displays a PCE of 6.2%, whereas the device fabricated by the conventional electrolyte injection approach presents a PCE of only 5.5%.

Received: July 16, 2013
Accepted: August 26, 2013
Published: August 26, 2013

   dx.doi.org/10.1021/am402856z | *ACS Appl. Mater. Interfaces* 2013, 5, 8289−8293

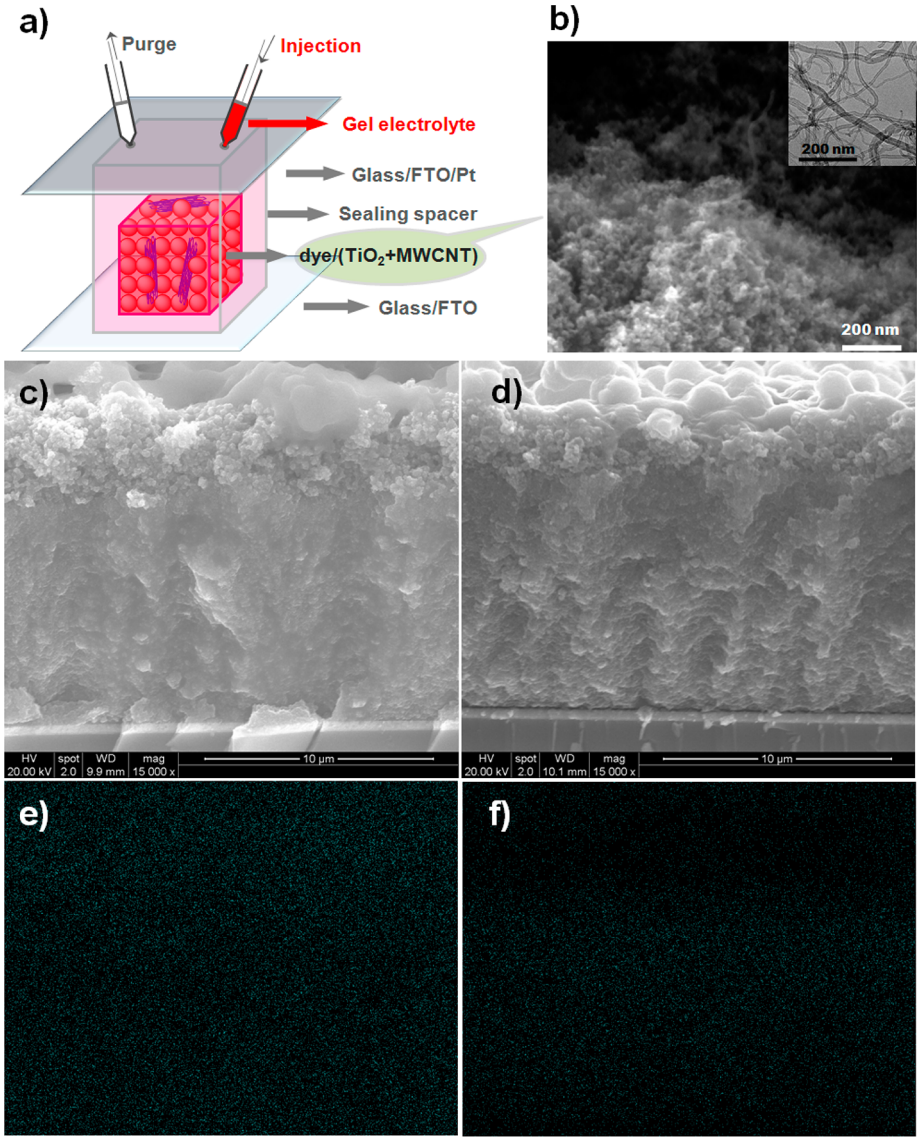

Figure 1. (a) Schematic illustration of device structures and gel electrolyte injection method, in which a purging process is performed when injecting gel electrolyte and MWCNT is incorporated into the TiO_2 nanoparticle-based anode to improve the charge and ion transport. (b) SEM image of the MWCNT/TiO_2 nanoparticle mixture for anode of quasi-solid-state dye-sensitized solar cells, inset showing the TEM image of the used MWCNT. (c, d) SEM images of the cross-sections of anode films filled with gel electrolyte, injection was performed in the presence (device **3**) and in the absence (device **7**) of air evacuation. (e, f) Element mapping of iodine of the cross sections of anode films of device **3** and **7**, respectively. Bright dots in e and f indicate the intensity of iodine in the cross-sections of device **3** and **7**, respectively.

For a systematic investigation, we begin our study from standard anode structure, i.e., one transparent layer and one scattering layer (ca. 12 μm of overall anode film thickness).[15] The gel electrolyte containing I_3^-/I^- as redox couple and poly(vinylidene fluoride-co-hexafluoropropylene) (PVdF-HFP) as supporting polymer is prepared according to the reported method with minor modifications.[10] By using the injecting-while-purging electrolyte filling method, the DSSC shows a PCE of 5.3% when using N719 as sensitizer, with short-circuit current density (J_{sc}) of 11.58 mA cm^{-2}, open-circuit voltage (V_{oc}) of 0.68 V and fill factor (FF) of 0.67 (device **1**, Figure 2). We then incorporate different amounts of MWCNT into TiO_2 anodes. An optimization shows that the weight percentage of MWCNT in TiO_2 paste at 0.00417% (device **2**) generates the highest efficiency of 5.8% (the detailed optimization process is provided in the Supporting Information). The device parameters are tabulated in Table 1 for easy comparison. It is observed that the improved PCE stems mainly from the increased FF, from 0.67 to 0.70, whereas the J_{sc} and V_{oc} show negligible improvement. This result is contradictory to that of liquid electrolyte based DSSC where the incorporation of MWCNT or graphene sheet usually lead to a considerable increase in J_{sc},[16−18] due to the enhanced charge collection efficiency. In quasi-solid-state DSSCs, the ion diffusion is a slow kinetics; the incorporation of MWCNT can facilitate the ion diffusion by forming well connected polymer gel electrolyte.[19,20] On the other hand, the existence of randomly distributed MWCNT would inhibit the crystallization of polymer gel in the anode films, whereas the amorphous phase can also generate a fast ion transport.[21] Because the FF of DSSC is associated with the total resistance of the device, the improvement in ion diffusion contributes to the FF enhancement in device **2**.

dx.doi.org/10.1021/am402856z | ACS Appl. Mater. Interfaces 2013, 5, 8289−8293

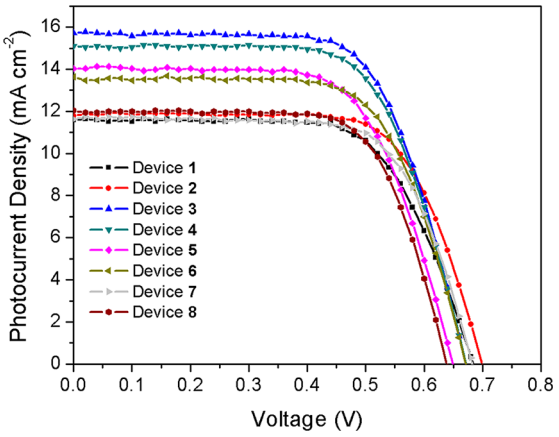

Figure 2. Photocurrent density–voltage characteristics of device **1** to **8**, measured under one sun illumination (AM 1.5G, 100 mW cm^{-2}).

Table 1. Device Structures and Photovoltaic Parameters of the Quasi-solid-state Dye-Sensitized Solar Cells Measured under 1 sun Illumination (AM 1.5 G, 100 mW cm^{-2})

DSSC[a]	MWCNT %[b]	film (μm)[e]	V_{oc}(V)	J_{sc} (mA/cm^2)	FF	PCE (%)
1	0	12	0.68	11.58	0.67	5.3
2	0.00417	12	0.70	11.79	0.70	5.8
3	0.00417	18	0.67	15.75	0.67	7.1
4	0.00417	23	0.67	15.10	0.67	6.8
5	0.00417	29	0.65	14.03	0.66	6.0
6	0	18	0.67	13.62	0.67	6.1
7	0.00417[c]	18	0.68	11.63	0.69	5.5
8	0.00417[d]	18	0.64	10.92	0.70	4.9

[a]The effective areas of all the devices are 0.196 cm^2. [b]The weight percentage of multiwalled carbon nanotube in the TiO_2 paste. [c]Injection of the gel electrolyte in the absence of air purging, other devices are fabricated adopting the injecting-while-purging electrolyte injection method. [d]Baking at 90 °C for 30 min. [e]Anode film thickness.

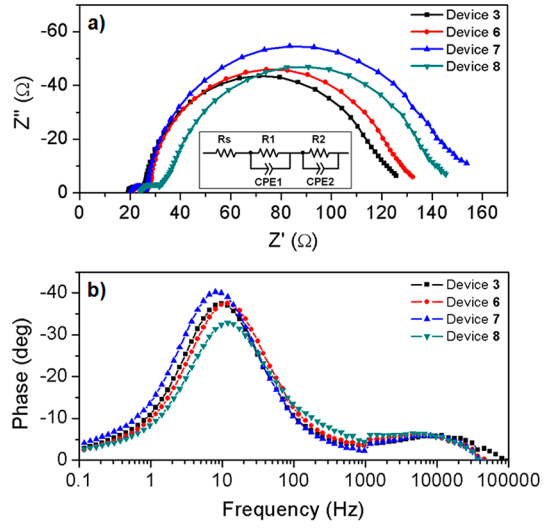

Figure 3. Electrochemical analysis of devices. (a) Nyquist and (b) Bode phase plots of device **3**, **6**, **7**, and **8**; the inset in (a) shows the equivalent circuit of the devices.

In quest of highly efficient DSSCs, development of dye molecules with broad spectral response in the full-visible to near-infrared region is one of the prerequisites. However, so far

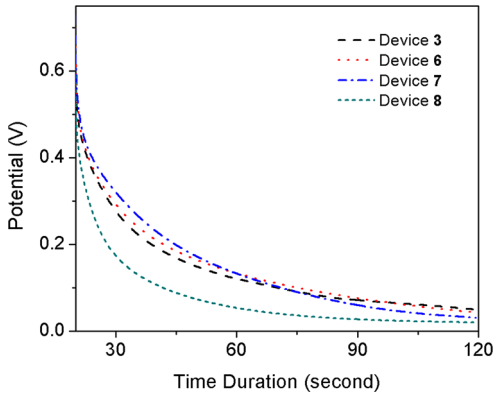

Figure 4. Open-circuit voltage decay profiles of device **3**, **6**, **7**, and **8**.

there is no dye possessing high extinction coefficient throughout the range due to synthetic barriers in molecular preparation.[8,9] A practical way to achieve attainable efficiency is to uptake more dye molecules by increasing the surface area of anode. In this context, we fabricate devices with film thickness up to 18 (device **3**), 23 (device **4**), and 29 μm (device **5**) using the optimized MWCNT/TiO_2 paste to increase the anode area. As a result, the DSSCs show PCEs of 7.1, 6.8, and 6.0%, respectively. The efficiency improvement is mainly due to the improved J_{sc}, from 11.79 mA cm^{-2} to 15.05, 15.10, and 14.03 mA cm^{-2} (Table 1 and Figure 2), which is consistent with the evolution of external quantum efficiency (EQE) of the devices (see Figure S1 in the Supporting Information). The improved light harvesting efficiency and charge collection efficiency contribute to the improvement in photocurrent conversion efficiency. The PCE decrease in device **4** and **5** is due to the progressively increased charge recombination probability induced by the increased electron percolation path length in thick anode films,[15] so that the MWCNT improved charge transport no longer significantly prevails over the back reaction with I_3^- species. The device based on pure TiO_2 nanoparticles also shows the highest efficiency of 6.2% when the film thickness is 18 μm (Table 1 and Figure 2, device **6**).

Electrochemical impedance spectroscopy (EIS) under dark at open-circuit voltage is studied to elucidate the charge transfer properties of the devices. There are two semicircles observed in the plots (Figure 3a), the equivalent circuit is shown as inset in Figure 3a. The smaller arcs in each spectrum correspond to the charge transfer resistance (R_1) at counter electrode. They are nearly the same because identical counter electrodes are applied. R_s is associated with sheet resistance. The larger arcs suggest the charge transfer resistance (R_2) from the conduction band of TiO_2 to electrolyte. In the absence of MWCNT incorporation (device **6**), the R_2 is calculated to be 98.4 Ω. With MWCNT incorporation (device **3**), the R_2 is reduced to 95.9 Ω. The decreased R_2 is due to the good conductivity of MWCNT which enables a fast charge transfer to electrolyte in the TiO_2 nanoparticle network.[22,23]

We thus perform comparison between our method and the conventional electrolyte injection method, i.e. in the absence of air evacuation (device **7**). The anode and cathode structures of the two devices are the same. As a consequence, device **7** shows an efficiency of 5.5%, which is considerably lower than that using injecting-while-purging electrolyte infiltration approach (7.1%). From Table 1 and Figure 2, the efficiency decrement originates mainly from the decreased J_{sc}, from 15.75 to 11.63 mA cm^{-2}. To explore the enhancement mechanism, we

dx.doi.org/10.1021/am402856z | ACS Appl. Mater. Interfaces 2013, 5, 8289–8293

conducted scanning electronic microscopy (SEM) characterizations of the anode films to investigate the pore filling behavior in the presence and in the absence of air evacuation. Device **3** shows a smoother cross-section image than that of device **7** (Figure 1c, d), indicting a more efficient electrolyte infiltration into the mesporous TiO_2 network with air evacuation. Furthermore, the element mapping of the anode films based on iodine is conducted (Figure 1e, f). First, it can be seen that the distribution of iodine in the anode of device **3** is more uniform than that in device **7**. In addition, the iodine content in device **3** is significantly higher than that in device **7**. Energy-dispersive X-ray spectroscopy (EDX) characterization (see Figure S2 in the Supporting Information) shows that the atomic percentage of iodine in the film of device **3** is around 6.9%, whereas that in device **7** is only about 4.2%. All of these evidences suggest that the pore filling of quasi-solid-state electrolyte is more efficient in the presence of air purging. Apparently, a high-degree of pore filling would generate fast ion (I^-/I_3^-) transport,[24] good wettability, and more efficient dye regeneration, thus leading to a high energy conversion efficiency of the quasi-solid-state DSSC. On the ground of EIS characteristics (Figure 3a), R_2 of device **7** is estimated to be 123.5 Ω, significantly larger than that of device **3**. Because the electrode structures of the two devices are identical in terms of dye-adsorbed TiO_2 nanoparticle networks, the retarded charge transfer is most likely due to the reduced contact area between TiO_2 and gel electrolyte, which results from the less efficient electrolyte infiltration. This effect in turn results in a portion of dye molecules becoming inactive that gives rise to smaller J_{sc}.

To increase the pore filling throughout the oxide network, a commonly used method is to bake the poorly wetted electrode at high temperature, usually 90 °C, for a period of time.[25] We compare this method with our approach by using the same electrode structures as device **3**. After the electrolyte injection (in the absence of purging), we bake the device at 90 °C for 30 min (device **8**), it turns out that the device efficiency is dropped to 4.9%. From Table 1, one can observe that the J_{sc} and V_{oc} are significantly decreased when compared with those of device **3**. However, the FF is increased from 0.67 to 0.70, indicating that the high temperature annealing would improve the cross-linking network of polymer skeleton and thus reduce the I_3^-/I^- diffusion impedance. However, this improvement is annihilated by significantly decreased J_{sc} and V_{oc} in terms of the overall device efficiency, most likely owing to the thermal damage of dye molecules since N719 becomes unstable when the device temperature exceeds 85 °C.[26] Furthermore, shorter baking time (10 min) could alleviate the damage, whereas the device efficiency (5.3%, see Figure S3 in the Supporting Information) is still significantly lower than that of device **3**. Therefore, our method based on kinetically driven electrolyte infiltration and wetting is advantageous when compared with thermal-driven pore filling method. Electrochemical analysis shows that the R_2 of device **8** is 109.2 Ω (Figure 3a), which is smaller than that of device **7**, indicating that the baking can indeed improve the wetting of electrolyte.

From the Bode phase plots of the devices (Figure 3b), the characteristic charge transfer frequencies (f) are obtained, which correspond to the peaks of the Bode phase plots. The higher frequency indicates a fast charge transfer process.[27] The peak frequencies of device **3**, **6**, **7**, and **8** are 9.6, 11.5, 8.3, and 12.2 Hz, respectively. It can be seen that the charge transfer from conduction band of TiO_2 to electrolyte is greatly blocked in device **7**, which is also an indication of less efficient pore filling between electrolyte and TiO_2 surface. While in device **3**, **6**, and **8**, with either purging or postbaking of the device at high temperature, the charge transfer becomes more efficient. In addition, MWCNT (O. D. × L = 6–9 nm × 5 μm of 3–6 layers) in the network reduces the percentage of TiO_2 nanoparticles in the anodes, which induces the smaller f of device **3** when compared with that of device **6**. The f of device **8** shows the highest value, suggesting the better contact between TiO_2 surface and the gel electrolyte for fast charge transfer.

To further probe the recombination kinetics of the devices, open-circuit voltage decay (OCVD) is recorded to illustrate the lifetime of V_{oc} from a steady state to dark equilibrium. Figure 4 shows the OCVD profiles of devices **3**, **6**, **7**, and **8**. The correlation between V_{oc} decay and electron lifetime (τ_n) can be described by eq 1

$$\tau_n = -\frac{K_B T}{e}\left(\frac{dV_{oc}}{dt}\right)^{-1} \quad (1)$$

where k_B is the Boltzmann constant, T is temperature, and e is the electron charge.[28,29] The electron lifetimes can be extracted from the slope of V_{oc} decay curve at initial stages. First, the decay curves of device **3** is similar to that of device **6**, indicating that the electron life is comparable. Notably, the photovoltage decay of device **7** is the slowest one. This is consistent with the electrochemical analysis that the poor wetting of dye/TiO_2 surface impede the back charge transfer, whereas the postannealing generates good wettability, which leads to the fastest voltage decay in device **8**.

In conclusion, we have developed an effective approach to infiltrate gel electrolyte in the mesoporous anode network for high performance quasi-solid-state DSSCs. This method avoids the high-temperature annealing that usually causes degradation of dye molecules. Additionally, the incorporation of carbon nanotubes can enhance the charge transport and thus allows the use of thick anode films for higher dye loading capacity and more efficient light harvesting. These two advancements finally lead to an impressive energy conversion efficiency of 7.1%, which is higher than both the conventional electrolyte injection method prepared device and solely TiO_2 nanoparticle anode based device. Our initial stability testing shows that the device efficiency maintains nearly the same after storage for 100 h (see Figure S4 in the Supporting Information). Because dye-sensitized mesoporous TiO_2 network is mostly applied for the devices, the proposed method would generate broad interests in the fabrication of high-efficiency devices with respective to different gel electrolytes and dye molecules. Finally, our method is feasible and easy to scale up for large area device fabrication when compared with the conventional infiltration methods.

■ ASSOCIATED CONTENT

Ⓢ Supporting Information

Detail of experiment including chemicals, instrumentations, and related experimental results. This material is available free of charge via the Internet at http://pubs.acs.org.

■ AUTHOR INFORMATION

Corresponding Author

*E-mail: taochen@phy.cuhk.edu.hk.

Notes

The authors declare no competing financial interest.

■ ACKNOWLEDGMENTS

The authors acknowledge the financial support from the CUHK Group Research Scheme and CUHK Focused Scheme B Grant "Center for Solar Energy Research". T. Chen acknowledges the University Research Grant (2060437). Q. Li acknowledges the support from GRF of RGC under project No. 414710.

■ REFERENCES

(1) Hagfeldt, A.; Boschloo, G.; Sun, L.; Kloo, L.; Pettersson, H. *Chem. Rev.* **2010**, *110*, 6595−6663.
(2) Goncalves, L. M.; Bermudez, V. D.; Ribeiro, H. A.; Mendes, A. M. *Energy Environ. Sci.* **2008**, *1*, 655−667.
(3) Kwon, Y. S.; Song, I.; Lim, J. C.; Song, I. Y.; Siva, A.; Park, T. *ACS Appl. Mater. Interfaces* **2012**, *4*, 3141−3147.
(4) Hamann, T. W.; Ondersma, J. W. *Energy Environ. Sci.* **2011**, *4*, 370−381.
(5) Nazeeruddin, M. K.; De Angelis, F.; Fantacci, S.; Selloni, A.; Viscardi, G.; Liska, P.; Ito, S.; Takeru, B.; Grätzel, M. *J. Am. Chem. Soc.* **2005**, *127*, 16835−16847.
(6) Yella, A.; Lee, H. W.; Tsao, H. N.; Yi, C. Y.; Chandiran, A. K.; Nazeeruddin, M. K.; Diau, E. W. G.; Yeh, C. Y.; Zakeeruddin, S. M.; Gratzel, M. *Science* **2011**, *334*, 629−634.
(7) Gratzel, M. *Acc. Chem. Res.* **2009**, *42*, 1788−1798.
(8) Li, L.-L.; Diau, E. W.-G. *Chem. Soc. Rev.* **2013**, *42*, 291−304.
(9) Hamann, T. W.; Jensen, R. A.; Martinson, A. B. F.; Van Ryswyk, H.; Hupp, J. T. *Energy Environ. Sci.* **2008**, *1*, 66−78.
(10) Wang, P.; Zakeeruddin, S. M.; Moser, J. E.; Nazeeruddin, M. K.; Sekiguchi, T.; Gratzel, M. *Nat. Mater.* **2003**, *2*, 402−407.
(11) Huo, Z.; Zhang, C.; Fang, X.; Cai, M.; Dai, S.; Wang, K. *J. Power Sources* **2010**, *195*, 4384−4390.
(12) Shi, Y.; Zhu, C.; Wang, L.; Zhao, C.; Li, W.; Fung, K. K.; Ma, T.; Hagfeldt, A.; Wang, N. *Chem. Mater.* **2013**, *25*, 1000−1012.
(13) Kubo, W.; Kitamura, T.; Hanabusa, K.; Wada, Y.; Yanagida, S. *Chem. Commun.* **2002**, 374−375.
(14) Kubo, W.; Murakoshi, K.; Kitamura, T.; Yoshida, S.; Haruki, M.; Hanabusa, K.; Shirai, H.; Wada, Y.; Yanagida, S. *J. Phys. Chem. B* **2001**, *105*, 12809−12815.
(15) Ito, S.; Murakami, T. N.; Comte, P.; Liska, P.; Grätzel, C.; Nazeeruddin, M. K.; Grätzel, M. *Thin Solid Films* **2008**, *516*, 4613−4619.
(16) Sun, S. R.; Gao, L.; Liu, Y. Q. *Appl. Phys. Lett.* **2010**, 96.
(17) Muduli, S.; Lee, W.; Dhas, V.; Mujawar, S.; Dubey, M.; Vijayamohanan, K.; Han, S. H.; Ogale, S. *ACS Appl. Mater. Interfaces* **2009**, *1*, 2030−2035.
(18) Yang, N. L.; Zhai, J.; Wang, D.; Chen, Y. S.; Jiang, L. *ACS Nano* **2010**, *4*, 887−894.
(19) Usui, H.; Matsui, H.; Tanabe, N.; Yanagida, S. *J. Photochem. Photobiol., A* **2004**, *164*, 97−101.
(20) Wang, P.; Zakeeruddin, S. M.; Comte, P.; Exnar, I.; Grätzel, M. *J. Am. Chem. Soc.* **2003**, *125*, 1166−1167.
(21) Croce, F.; Appetecchi, G. B.; Persi, L.; Scrosati, B. *Nature* **1998**, *394*, 456−458.
(22) Sawatsuk, T.; Chindaduang, A.; Sae-Kung, C.; Pratontep, S.; Tumcharern, G. *Diamond Relat. Mater.* **2009**, *18*, 524−527.
(23) Yang, L.; Leung, W. W.-F. *Adv. Mater.* **2013**, *25*, 1792−1795.
(24) Nguyen, T.; Wang, X. *J. Power Sources* **2010**, *195*, 1024−1030.
(25) Shi, Y.; Wang, K.; Du, Y.; Zhang, H.; Gu, J.; Zhu, C.; Wang, L.; Guo, W.; Hagfeldt, A.; Wang, N.; Ma, T. *Adv. Mater.* **2013**, *25*, 4413−4419.
(26) Asghar, M. I.; Miettunen, K.; Halme, J.; Vahermaa, P.; Toivola, M.; Aitola, K.; Lund, P. *Energy Environ. Sci.* **2010**, *3*, 418−426.
(27) Hsing, I. M.; Wang, X.; Leng, Y. J. *J. Electrochem. Soc.* **2002**, *149*, A615−A621.
(28) Bisquert, J.; Zaban, A.; Greenshtein, M.; Mora-Seró, I. *J. Am. Chem. Soc.* **2004**, *126*, 13550−13559.
(29) Zaban, A.; Greenshtein, M.; Bisquert, J. *ChemPhysChem* **2003**, *4*, 859−864.